




Sprayed Ag oxygen reduction reaction gas-diffusion electrodes for the electrocatalytic reduction of CO₂ to CO

Patrick Wilde¹ | Anil Özden¹ | Henrik Winter¹ | Thomas Quast¹ |
 Jonas Weidner¹ | Stefan Dieckhöfer¹ | João R. C. Junqueira¹  |
 Matthias Metzner³ | Willi Peter³ | Werner Leske³ | Denis Öhl¹ |
 Tim Bobrowski¹ | Thomas Turek² | Wolfgang Schuhmann¹  

¹Analytical Chemistry—Center for Electrochemical Sciences (CES), Faculty of Chemistry and Biochemistry, Ruhr University Bochum, Bochum, Germany

²Institute of Chemical and Electrochemical Process Engineering, Clausthal University of Technology, Clausthal-Zellerfeld, Germany

³Performance Colors & Glass, Performance Coatings, Ferro GmbH, Frankfurt/Main, Germany

Correspondence

Wolfgang Schuhmann, Analytical Chemistry—Center for Electrochemical Sciences (CES), Faculty of Chemistry and Biochemistry, Ruhr University Bochum, Universitätsstr. 150, D-44780 Bochum, Germany.
 Email: wolfgang.schuhmann@rub.de

Funding information

H2020 European Research Council, Grant/Award Number: 833408; Deutsche Forschungsgemeinschaft; Bundesministerium für Bildung und Forschung, Grant/Award Number: 033RC017E

Abstract

Gas-diffusion electrodes have been successfully employed in electrochemical chlorine production, and they also hold great potential in the field of electrochemical CO₂ reduction. Herein, we demonstrate how sprayed Ag-based gas-diffusion electrodes, which show outstanding performance for the reduction of oxygen, need to be modified to produce CO from CO₂. A computer-controlled automated airbrush-type spraying setup is used to systematically vary the core fabrication parameters of the process and investigate their effect on the electrochemical performance. Focused ion-beam milling combined with scanning electron microscopy provides deeper insight into the structure of the electrodes and serves in combination with electrochemical data as the measure for the optimisation. Eventually, electrodes can be produced that suppress the evolution of H₂ to the extent that an average Faradaic efficiency of 79% for CO can be maintained for at least 10 h at a current density of $-100 \text{ mA}\cdot\text{cm}^{-2}$.

KEYWORDS

Ag powder, automated spray-coater, CO₂RR, carbon monoxide, gas diffusion electrodes

1 | INTRODUCTION

The efficient conversion of electric into chemical energy via electrochemical reactions presents a feasible way to tackle the challenges that arise from the finite nature of fossil resources [1]. Such reactions allow for the generation of 'green' hydrogen as a clean fuel through electrochemical water splitting or the reduction of the waste molecule CO₂ to

valuable chemical feedstock via the electrochemical CO₂ reduction reaction (CO₂RR) [2]. CO is undoubtedly one of the reaction's most interesting products since it finds wide application in Fischer–Tropsch synthesis, where it constitutes one of the two key components of syngas along with hydrogen [3]. One of the major challenges in the CO₂RR, however, is to supply the catalytically active sites with the reactant CO₂, since its solubility in the aqueous electrolyte is limited to around 30 mM

This is an open access article under the terms of the Creative Commons Attribution-NonCommercial-NoDerivs License, which permits use and distribution in any medium, provided the original work is properly cited, the use is non-commercial and no modifications or adaptations are made.

© 2022 The Authors. *Applied Research* published by Wiley-VCH GmbH.

under ambient conditions [3]. On the one hand, KOH solutions, which typically exhibit pH-values above 12, beneficially suppress the parasitic hydrogen evolution reaction (HER), but on the other hand, they prevent sufficiently high CO₂ concentrations that are required for high current density due to the formation of insoluble carbonate species [4]. The use of gas-diffusion electrodes (GDEs) is considered a possible solution to this challenge because they provide the gaseous reactant in close proximity to the reaction zone.

GDEs are already applied for different electrochemical reactions like the hydrogen oxidation reaction [5], nitrogen reduction reaction [6], oxygen reduction reaction (ORR) [7], and also the CO₂RR [8]. Within a GDE, double- or triple-phase boundaries are formed (TPB) [9, 10], where either all three phases are in direct contact with each other, or where extremely thin liquid layers (0.01–1 μm) [10] cover the catalyst material in the presence of the gaseous reactant [11]. Compared to conventional electrolysis cells with diffusion path lengths of 60–160 μm [12], which operate in a diffusion-limited regime and are therefore restricted to an operation between –35 and –100 mA·cm^{–2} [11]. The diffusion path lengths of the CO₂ molecules to the catalytically active sites are significantly shorter in GDEs, leading to increased mass transport of reactants to and products away from the active centres and enabling current densities of up to several hundreds of mA·cm^{–2}. They also reduce the rate of carbonate precipitation and allow for the use of alkaline electrolytes in the CO₂RR.

Since Ag is a suitable catalyst for the reduction of CO₂ to CO with high Faradaic efficiencies (FEs) of more than 90% [13], Ag GDEs were successfully applied [14]. On the industrial scale, the electrodes are prepared via a dry process, where the catalyst component is mixed with a binder, spread across a conductive current collector, and pressed with the help of rolling mills [15]. On a smaller scale, the preparation of Ag GDEs can also be successfully realised via a wet spraying approach. An Ag-containing suspension is sprayed together with a pore-forming agent and polytetrafluoroethylene (PTFE) onto a metal mesh, which is then compressed and heated [16, 17].

In this study, we demonstrate how the fabrication of Ag GDEs can be modified to adapt the properties, which were initially optimised for the ORR, to the electrocatalytic reduction of CO₂ to CO. By systematically changing the fabrication parameters such as the number of the sprayed layers, the applied pressure, the nature of the Ag material, the PTFE content a gradual shift towards an Ag GDE for the CO₂RR was achieved.

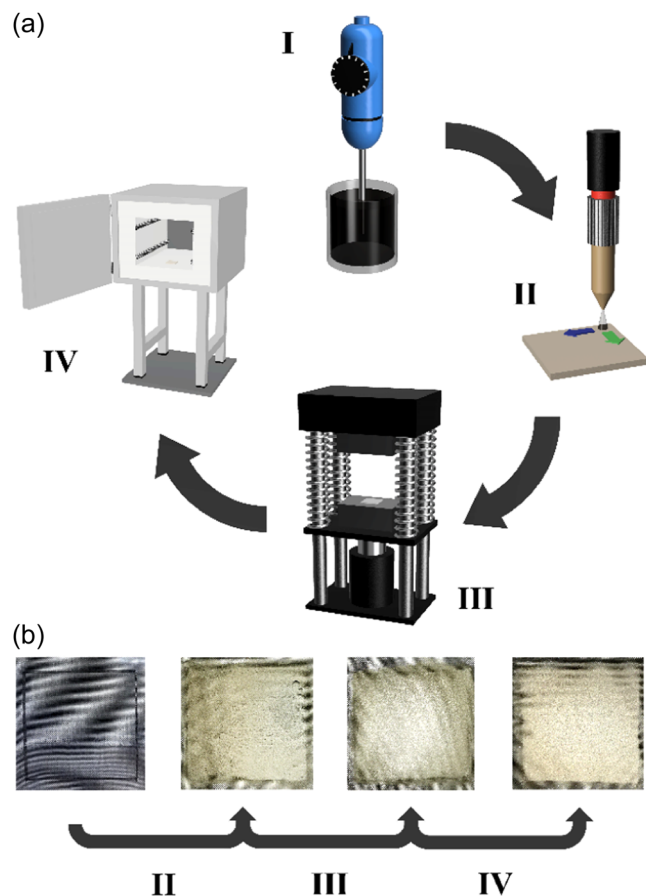
2 | EXPERIMENTAL SECTION

The standard procedure for the preparation of the spraying suspension was according to the following protocol. First, 4.46 ml of deionised water was mixed with 3.33 g of Ag-base material (*Ferro*) and 5.56 g of a 1% methyl-cellulose (*Sigma Aldrich*) solution. After the addition of another 10 ml of deionised water the ink was stirred with a *T10 Ultra-Turrax* (*IKA*) equipped with a *S10N-5G* tool (*IKA*) for a total duration of 95 min. The *Ultra-Turrax* worked at an interval of 5 min 'on' followed by 10 min 'off', which adds up to total 'on'-time of 35 min.

Subsequently, 0.175 g of *Dyneon* PTFE dispersion (3M), was added as well as 10 ml of deionised water. The latter could also be replaced by 10 ml of isopropanol for improved spraying. Then, the suspension was left to stir with a magnetic stirring bar for an additional 35 min before it could be sprayed. For the spraying process, a piece of 3 × 3 cm² of either Ni-(56 μm mesh width from *Haver & Boecker*) or PEEK-mesh (PK-100/34 from *Franz Eckert*) was cut and placed on a heating plate at 220°C. The computer-controlled sprayer was programmed to fully cover an area of 2.2 × 2.2 cm² with an increment of 2 mm to produce one layer. At each position either 18 or 14 μl of suspension were dispensed at a rate of 15 μl·s^{–1}. In between each spot a delay of 2 s was added to allow the ink to dry. The pressure for the air brush system was 1.5 bar. After the completed spraying process, the electrode was pressed with a hydraulic press (*Graveda Graspreso Epic 15T*) between two steel plates at 130°C and with pressures of either 60, 100, or 160 bar for 5 min. Subsequently, the pressed electrode was placed in an oven (*Nabertherm*), which was heated up for 150 min until a maximum temperature of 330°C was reached, which was held for 10 min. After that, the oven was left to cool down to room temperature overnight before the electrode was removed. A circular electrode with a diameter of 18 mm was cut out of the final square electrode and placed between two 3D-printed TPU rings. The sandwich structure was pressed at very light pressure at 213°C until both rings were melted together and formed one solid structure. Potential gaps were closed by melting the region with a soldering tip (Supporting Information: Figure S5). The exposed circular surface of the electrode had a diameter of 12 mm. The whole step was carried out to avoid the lateral diffusion of gases out of the electrochemical cell. SEM images were taken, and focused ion beam (FIB) milling was performed using a *Quanta 3D FEG SEM* operated at 20.0 kV. Electrochemical measurements were performed using a *Metrohm Autolab PGSTAT302N* or a *Biologic VMP3* in a 3-electrode cell setup with a *Fumatech FAB-PK-75* anion exchange membrane that separated anode and cathode compartment (Supporting Information: Figure S6). A Ni-mesh electrode served as counter electrode, a Ag|AgCl|3M KCl was used as reference electrode together with a double junction to avoid contamination of the catholyte. Chronoamperometry measurements were recorded for 1 h at four different current densities (15 min each) or for 10 h at –100 mA·cm^{–2}. Gas samples were taken every 7.5 min from either top or bottom compartment in turns and automatically injected into an online-coupled gas chromatograph. The gas stream, which was injected into the gas chromatograph was selected using either a manual 6-way valve (*Swagelok*) or an automatic 6-way valve (*Machery-Nagel*). Gas products were analysed using an *SRI 8610C multiple gas analyzer #5* gas chromatograph from *SRI Instruments*.

3 | RESULTS AND DISCUSSION

The preparation procedure of the GDEs was adapted from a previously published method (Scheme 1) [16, 17]. Briefly, the spraying suspension was prepared through adding the respective



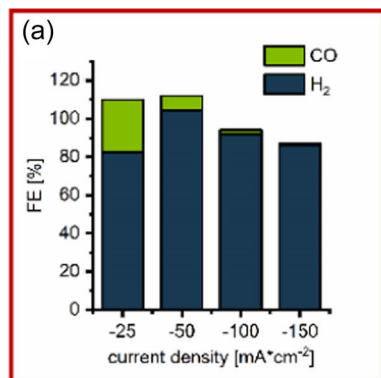
SCHEME 1 Fabrication process of sprayed Ag-GDEs starting with the Ultra-Turrax-assisted preparation of the spray suspension (I) followed by the automated spraying process with a computer and step-motor-controlled custom-made air-brush nozzle (II), the tempered pressing procedure (III), and the final heating step in a furnace under ambient atmosphere (IV) in (a). Photographs of the Ag-GDEs at the different stages of the fabrication process (b). GDE, gas-diffusion electrode.

Ag material, methylcellulose solution, water, and PTFE together with an Ultra-Turrax. Subsequently, the suspensions were sprayed onto a Ni-mesh by means of an automated airbrush-type spraying setup. The obtained films were then pressed with a hot-press before a final heating step under ambient atmosphere yielding the functional gas diffusion electrodes. This multistep process opens a large parameter space and creates a complex optimisation problem.

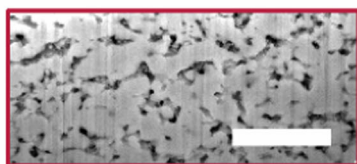
Therefore, the initial electrode was made following a recipe, which was developed for the fabrication of Ag GDEs for the reduction of oxygen and adapted to the given lab equipment and most specifically to the automated spraying system [16,17]. When the Ag GDE (Ag powder 372) is used for the CO₂RR both CO and H₂ are produced as expected (Figure 1a). However, the major product is H₂, whereas CO only accounts for 27% at -25 mA·cm⁻² down to 1% at -150 mA·cm⁻² FE. The results indicate that even though CO₂RR occurs on the GDE, the system does not reach the predominant selectivity for CO.

This is not astonishing since in the case of the ORR no competing reduction reaction can occur. Hence, the location of the TPB within the GDE is supposedly much less important than in the case of the CO₂RR where any electrolyte-wetted electrode surface may preferentially evolve H₂. We hence propose that the TPB in the case of the CO₂RR should be located as close as possible to the interface between GDE and electrolyte, which evidently requires an adaptation of the electrode structure to mitigate potential-induced wetting and to allow the penetration of the gaseous CO₂ through nearly the complete GDE thickness. Since the performance of a GDE greatly depends on the properties of the pore system (e.g., hydrophobicity, surface area, conductivity, and pore shape), different ways to modify these are investigated. Major modifications were performed in terms of changing (i) the PTFE content and type of PTFE modification, (ii) the applied pressure, (iii) the spraying parameters, and (iv) the nature of the Ag material. Modifying the amount of PTFE, which is placed inside or on top of the GDE is expected to affect the wettability or in other words the degree to which the electrolyte can penetrate into the pore system [18]. Both, completely flooded and dry electrodes (as the most extreme examples) are expected to decrease the CO₂RR efficiency due to the dominance of the parasitic HER [19]. Whereas flooded GDEs are enhancing the HER since their channels are blocked for CO₂, dry GDEs promote the HER due to the lack of an efficient TPB and thereby lack of an efficient CO₂RR.

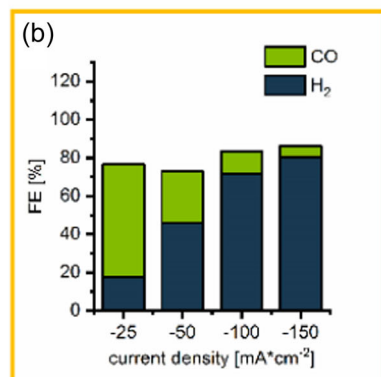
Neither the increase of the PTFE content inside the GDE by a factor of 5 nor the decrease of PTFE by half had a beneficial effect on the performance of the GDE (Supporting Information: Figure S1). The PTFE increase led to the complete loss of the functionality of the GDE with H₂ being the only detectable product, whereas the decrease of PTFE produced CO with only a FE of 3% at -150 mA·cm⁻². The hydrophobicity of the electrode surface was further tuned through the addition of PTFE after the initial spraying process, which was either drop-coated (113 μl of a 1 mg·ml⁻¹ PTFE suspension in ethanol) or sprayed as an additional layer (spraying suspension without the addition of Ag powder) on top of the GDE before the final heating step (Scheme 1 IV). These modifications did also not increase the selectivity for CO (3% and 6% FE for CO at -150 mA·cm⁻²). Thus, the wettability of the electrode does not seem to be the main bottleneck for an improved electrochemical performance of the sprayed Ag GDEs. Furthermore, we investigated whether a decrease in pressure during the preparation (Scheme 1 III) can modulate the porosity and the size of the channels and thus provide not only a larger volume of the TPB but also improve CO₂ mass transport towards the reaction zone. Decreasing the pressure from 160 to 100 bar and 60 bar shows a significant effect on the product distribution. Whereas an electrode pressed at 160 bar shows FEs for CO between 27% and 1% for current densities between -25 and -150 mA·cm⁻² (Figure 1a), a GDE fabricated at 100 bar shows a higher CO selectivity with FEs between 59% and 6% in the same current density range (Figure 1b). Further decrease of the pressure to 60 bar does not improve the performance further but comes at the expense of a decreased mechanical stability (CO FEs between 66% and 6%).



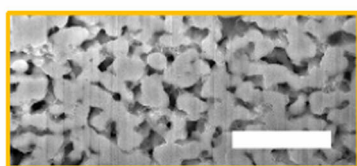
Ag powder 372, 160 bar



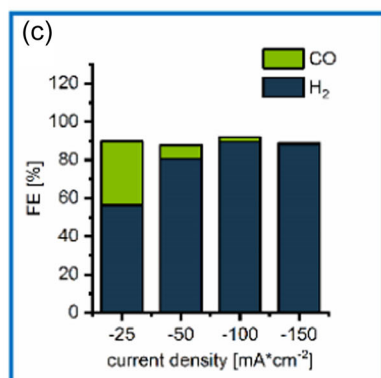
porosity: 29 %



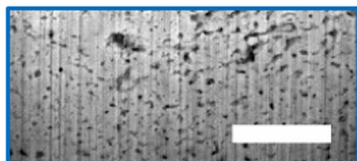
Ag powder 372, 100 bar



porosity: 39 %



Ag flakes D29, 100 bar



porosity: 12 %

FIGURE 1 CO₂RR performance of different Ag gas-diffusion electrodes. FEs are plotted for different current densities in mA·cm⁻² for CO (green) and H₂ (blue) in %. Ag powder 372 at 160 bar pressure (a) and 100 bar pressure (b) as well as Ag flakes D29 at 100 bar pressure were investigated. Corresponding FIB-milled cross-sections with a size of 35 × 15 μm². Porosity was derived using the ImageJ software. Scale bars equal 10 μm.

The cross-sections, which were obtained by FIB-milling of the as-prepared electrodes, provided insight into the different pore systems. The degree of porosity could be evaluated based on the visual assessment of the images, where the ratio between pixels that belong to the pore system and pixels that are part of the solid electrode material was determined. The cross-sections indicate a porosity of 39% for 100 bar pressure, which is 10% higher than for the 160 bar equivalent. Changing the Ag base material to Ag flakes (Ag flakes D29) created a denser film, which resulted in only 12% porosity and reflected in comparably poor electrochemical CO₂RR performance. FEs for CO started at 34% for -25 mA·cm⁻² but quickly decreased to 7% at -50 mA·cm⁻² and eventually dropped to 1% at the highest current density. These results underline the effect of the porosity and ultimately the Ag material of the GDE on its electrochemical CO₂RR performance. Based on these findings, the following electrodes were prepared using a pressure of 100 bar and the initial Ag powder.

Since larger pores inside a GDE create less transport barriers and hence less confinement of reaction species, it is expected that those electrodes exhibit an increased mass transport of CO₂ to and of CO and H₂ away from the reaction zone, which provides the basis for improved reaction dynamics [20].

The previous results raise the question how mass transport could be even further increased. One potential option lies in shorter diffusion pathways by reducing the thickness of the electrodes. Additionally, a reduction in thickness would automatically reduce the surface area in the flooded part of the electrode, which is not affecting the volume of the TPB but is predominantly available for HER only. Electrodes optimised for ORR do not need to consider this aspect due to less cathodic operation potentials, but it becomes highly relevant for the CO₂RR. By reducing the surface area where only HER can occur, FEs for CO are expected to increase. The automatic spraying setup allows to precisely control the amount of

the sprayed material (Scheme 1 II) and hence the thickness. The initial electrodes were sprayed with a total of eight layers (four on each side of the Ni-mesh) with 2 mm increments in x- and y-direction. At each position 18 μL of the suspension were dispensed. First, the number of sprayed layers was decreased to a total of four with two layers on each side of the Ni-mesh. These changes improved the CO₂RR significantly. The formation of CO was predominant at lower current densities of -25 and -50 $\text{mA}\cdot\text{cm}^{-2}$ with FEs for H₂ and CO of 10%–103% and 14%–94%, respectively. Total FEs of above 100% are the result of measurement inaccuracies of approximately $\pm 15\%$. The product selectivity then changed to FEs of 48%–48% and 67%–29% with H₂ as the major product at the higher current densities of -100 and -150 $\text{mA}\cdot\text{cm}^{-2}$ (Figure 2a). This raises the question, if the change at higher current densities is solely the consequence of potential-induced flooding [21] of the electrode or could also indicate a mass transport limitation of CO₂ to the reaction zone under increased product turnover. Therefore, the thickness was reduced even further by changing the total number of layers to three, with two layers on the side of the Ni-mesh facing the electrolyte and one layer on the gas-feed side of the mesh. The results confirm that the decreased thickness provides an improved performance at all current densities. The product range was dominated by CO with FEs for H₂ and CO of 6%–109%, 5%–108%, and 26%–74% at -25 , -50 ,

and -100 $\text{mA}\cdot\text{cm}^{-2}$, respectively. Only at -150 $\text{mA}\cdot\text{cm}^{-2}$ H₂ was the major product with a FE of 50 (Figure 2b). Further reduction of the number of Ag layers to two layers (one on each side of the Ni mesh) continued the trend (Figure 2c). To reduce the amount of sprayed Ag suspension even more, the dispense volume of the layer facing the gas feed side was decreased from 18 to 14 μL .

The performance of this electrode exceeds all previous electrodes (Figure 2d). For the first time the GDE produced CO as the major product throughout the whole range of current densities. FEs of 7%–103%, 5%–103%, 6%–97% and 17%–83% were obtained for current densities between -25 and -150 $\text{mA}\cdot\text{cm}^{-2}$. The electrode series (Figure 2a–d) clearly illustrates, how reducing the flooded volume that is available for HER only, leads to an increase in selectivity for CO. Whereas all electrodes perform relatively well at low current densities, it is especially true for thicker electrodes that the parasitic HER impairs the performance significantly at higher current densities and hence more cathodic potentials. Thinner electrodes, which offer less flooded electrode surface and thus deprive the HER of its basis, suffer much less from this effect as evidenced by the stepwise decrease of FE values for hydrogen at -150 $\text{mA}\cdot\text{cm}^{-2}$. We also attempted to spray only one single layer on the Ni-mesh side, which faces the electrolyte. Even though a continuous film could be obtained, the modification resulted in a steep decrease in CO₂RR efficiency

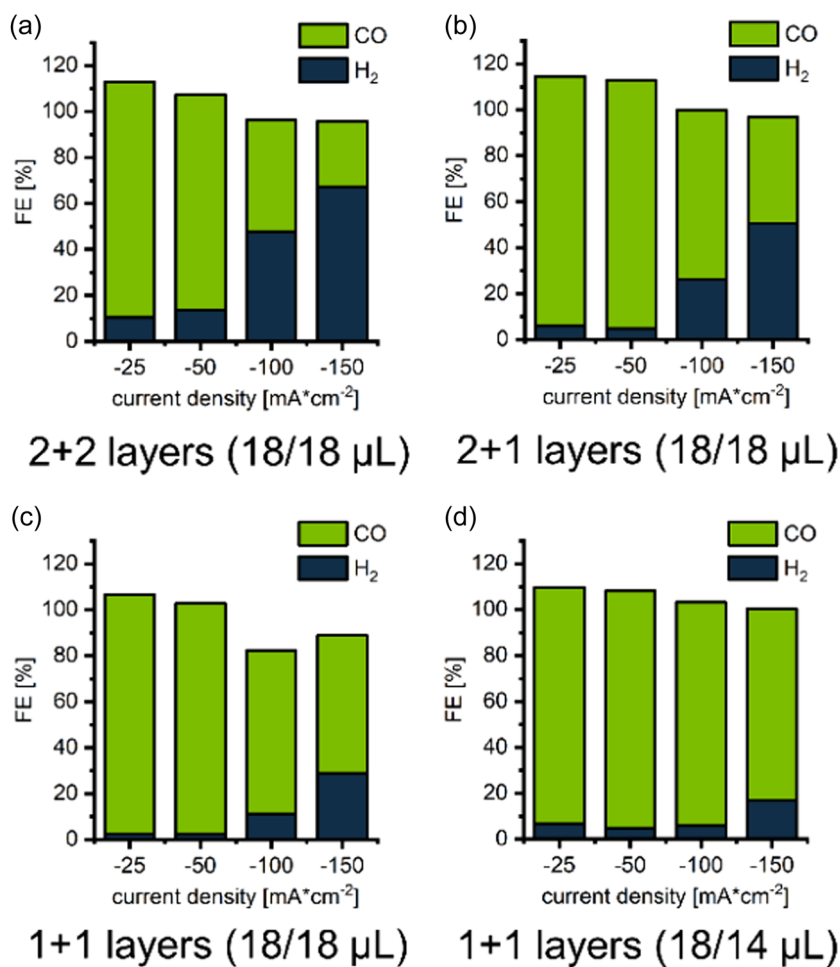


FIGURE 2 CO₂RR performance of different Ag gas-diffusion electrodes. FEs are plotted for different current densities in $\text{mA}\cdot\text{cm}^{-2}$ for CO (green) and H₂ (blue) in %. Different Ag layers with 18 μL dispense volume at each spraying location were investigated, 2 + 2 layers (a), 2 + 1 layers (b), 1 + 1 layers (c) and 1 + 1 layers with a reduced dispense volume of 14 μL for one layer (d). FE, Faradaic efficiency.

(Supporting Information: Figure S2). This becomes especially clear at $-150 \text{ mA}\cdot\text{cm}^{-2}$, where H_2 retakes the role as the major product. It can be hypothesised, that in case of a single Ag layer the Ni-mesh cannot be fully covered, and that the exposed Ni surface contributes to the overall reaction as an HER catalyst.

The observation raises the question to which extent the observed hydrogen evolution can be attributed to the Ni mesh as the current collector. Since Ag is electrically conductive by its metallic nature, it is possible to replace the Ni-mesh as the current collector by a nonconductive and chemically stable substrate. Electrochemically inert polyether ether ketone (PEEK) was investigated as a possible substitute (Supporting Information: Figure S3). The results reveal a performance with lower selectivity for CO compared to the electrode, which uses Ni-mesh (Figure 2d). More H_2 is produced with FEs for H_2 and CO of 48%–57% at $-150 \text{ mA}\cdot\text{cm}^{-2}$. Importantly, this result does not only indicate that the HER cannot be solely due to the catalytic activity of partially exposed Ni-mesh, but it suggests that it predominantly originates from the parasitic side reaction on the Ag GDE. The results clearly illustrate that in addition to the size of the channels and the porosity of the electrode, its thickness plays a major role in the electrochemical CO_2RR performance.

A trend that is still observable at this stage, however, is that the selectivity for CO decreases with increasing current densities and thus measurement time. Ideally, an Ag GDE would exhibit high selectivity for CO, which remains stable over prolonged periods of time and performs irrespectively of the applied current density. After the applied pressure during the fabrication and the number of sprayed layers was optimised and it was shown that the choice of the Ag material can have a significant effect on the performance of the electrode, one more change in material was made to achieve an improved selectivity over the whole range of applied current densities. Since flakes did not show promising pore-forming properties but the formation of a dense film (Figure 1c), another spherical Ag powder was used (Ag powder 328X). According to the physical specifications of the material, this powder exhibits a microcrystalline structure with a high and roughened surface area despite a comparably large particle size (Supporting Information: Figure S4). Both properties are typically beneficial for the electrocatalytic activity of a material. Additionally, since the tap density of $1.0\text{--}1.6 \text{ g}\cdot\text{cm}^{-3}$ of the Ag powder 328X is lower than the equivalent values of the Ag powder 372 ($1.2\text{--}1.7 \text{ g}\cdot\text{cm}^{-3}$) and much lower than the one of the Ag flakes D29 ($4.1\text{--}4.6 \text{ g}\cdot\text{cm}^{-3}$) it is expected that the resulting electrodes could also show a higher degree of porosity. The final electrode was sprayed with two layers and a dispense volume of $18 \mu\text{l}$ to ensure a continuous film. An SEM micrograph of its cross-section confirms the $50 \mu\text{m}$ diameter of the Ni-wire and shows that electrode thickness varies between $135 \mu\text{m}$ where the wires overlap and $90 \mu\text{m}$ in the gaps between the wires (Figure 3a).

The cross-section, which was obtained through FIB milling, reveals a slightly higher porosity of 41% with a clearly defined channel structure (Figure 3b). A significant improvement can be observed in terms of the electrochemical performance. The major difference to the previous electrodes lies in the fact, that the

electrode based on the Ag powder 328X improves its performance with increasing current densities. Where the initial FEs for H_2 and CO are 10%–101% at $-25 \text{ mA}\cdot\text{cm}^{-2}$, the selectivity for CO increases to FEs of 6%–105% at $-50 \text{ mA}\cdot\text{cm}^{-2}$, 3%–102% at $-100 \text{ mA}\cdot\text{cm}^{-2}$ and reaches 2%–84% at a current density of $-150 \text{ mA}\cdot\text{cm}^{-2}$. The obtained results show the beneficial properties of the 328X material for the Ag-GDE fabrication. To investigate the electrode performance in terms of stability, selectivity, and activity over a prolonged period of time, CO_2RR was performed for the duration of 10 h at a current density of $-100 \text{ mA}\cdot\text{cm}^{-2}$. The recorded potential of the working electrode shows a stable value of around -0.57 V versus reversible hydrogen electrode (Figure 4a) indicating not only a constant activity

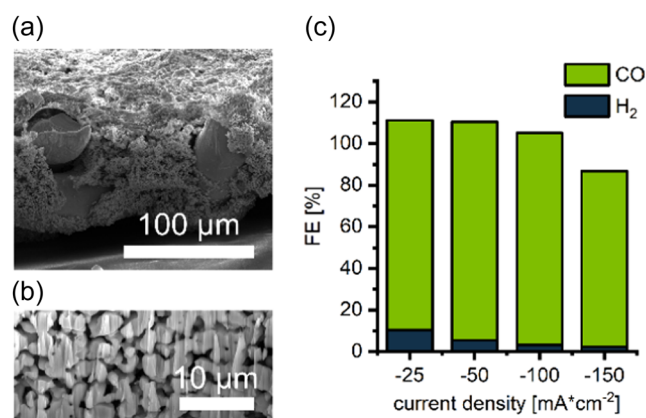


FIGURE 3 SEM micrographs of the cross-section through cutting (a) and FIB-milling (b). Electrochemical CO_2RR performance of the 328X-based Ag gas-diffusion electrode (c). FEs are plotted for different current densities in $\text{mA}\cdot\text{cm}^{-2}$ for CO (green) and H_2 (blue) in %.

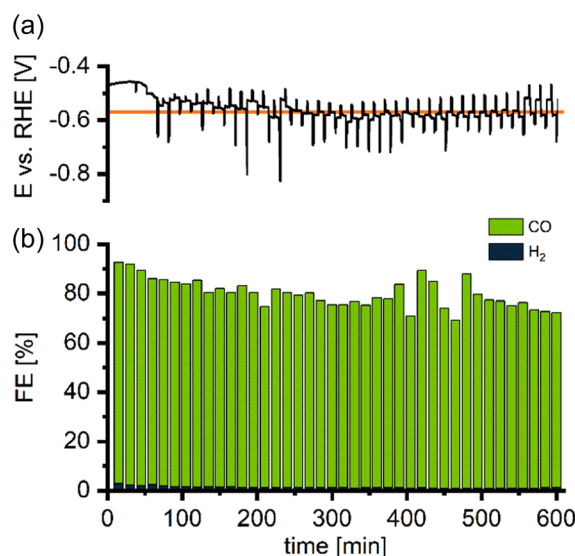


FIGURE 4 Ten hour electrochemical CO_2RR performance of the 328X-based Ag gas-diffusion electrode at $-100 \text{ mA}\cdot\text{cm}^{-2}$. The iR -corrected working electrode potential versus RHE in V (a) and FEs are plotted for different times in min for CO (green) and H_2 (blue) in % (b). Orange line serves as guide to the eye.

but also good mechanical as well as electrochemical stability. Fluctuation spikes in the potential profile are due to sudden pressure changes induced by the switching of an automatic valve that guides the gas stream of either the bottom or top compartment of the electrochemical cell to the gas chromatograph.

CO is the major product throughout the whole measurement. With an initial FE for CO of 90%, the measurement reconfirms the performance observed during the shorter measurement at $-100\text{ mA}\cdot\text{cm}^{-2}$. The change of the FEs in the following samples shows a slight decrease in the selectivity for CO to 71% after 600 min, which results in an average FE for CO of 79% over the course of the whole 10 h (Figure 4b). The experiment provides evidence for a stable electrode operation and in conclusion emphasises the importance of the optimisation process to enable a successful transfer of the GDE functionality from one electrochemical reaction to another. This is especially relevant, if the optimal reaction conditions depend on the porosity of the electrode as well as the mass transport of reactant and product species within the electrode, or, as for the CO_2RR reaction the possibility for a competitive parasitic reaction at the same electrode potentials.

4 | CONCLUSION

The adaption of the fabrication process of airbrush-sprayed Ag gas diffusion electrodes from the ORR to the electrochemical CO_2RR is demonstrated. The findings indicate that the controlled modification of the three core parameters (i) pressure, (ii) thickness, and (iii) nature of the Ag material can change the functionality and improve the performance of the electrodes significantly from initial predominantly H_2 -producing electrodes to efficient CO producing ones. The final electrodes exhibit high selectivity for CO, which remains stable over the course of 10 h with an average FE of 79%. The study underlines that gas diffusion electrodes need to be precisely tailored for the individual field of application before the desired performance can be achieved. Evidently, transferring knowledge from GDEs for the ORR to GDEs for the CO_2RR requires the consideration of different boundary conditions. In this context, the parasitic HER plays a major role. Increasing porosity and decreasing the thickness reduces the area of the electrode, which is not part of the TPB and is predominantly responsible for the HER. Consequently, the HER can be suppressed and a successful transfer of GDEs from ORR to CO_2RR is achieved.

ACKNOWLEDGEMENTS

Financial support by European Research Council (ERC) under the European Union's Horizon 2020 research and innovation programme (CasCat [833408]), the Deutsche Forschungsgemeinschaft (DFG) in the framework of the research unit FOR 2397 (276655237), and the BMBF in the framework of the project CO2-WIN: ProMet (033RC017E).

DATA AVAILABILITY STATEMENT

The data that support the findings of this study are available from the corresponding author upon reasonable request.

ORCID

João R. C. Junqueira  <http://orcid.org/0000-0003-1685-7861>

Wolfgang Schuhmann  <http://orcid.org/0000-0003-2916-5223>

TWITTER

Wolfgang Schuhmann  @ELAN_RUBSchuhmannLab

REFERENCES

- [1] I. Katsounaros, S. Cherevko, A. R. Zeradjanin, K. J. J. Mayrhofer, *Angew. Chem. Int. Ed.* **2014**, *53*, 102.
- [2] a) Z. W. Seh, J. Kibsgaard, C. F. Dickens, I. Chorkendorff, J. K. Nørskov, T. F. Jaramillo, *Science* **2017**, *355*, eaad4998.; b) R. Sharifian, R. M. Wagterveld, I. A. Digdaya, C. Xiang, D. A. Vermaas, *Energy Environ. Sci.* **2021**, *14*, 781.
- [3] S. Nitopi, E. Bertheussen, S. B. Scott, X. Liu, A. K. Engstfeld, S. Horch, B. Seger, I. E. L. Stephens, K. Chan, C. Hahn, J. K. Nørskov, T. F. Jaramillo, I. Chorkendorff, *Chem. Rev.* **2019**, *119*, 7610.
- [4] E. R. Cofell, U. O. Nwabara, S. S. Bhargava, D. E. Henckel, P. J. A. Kenis, *ACS Appl. Mater. Interfaces* **2021**, *13*, 15132.
- [5] P. Rodenas, F. Zhu, A. ter Heijne, T. Sleutels, M. Saakes, C. Buisman, *J. Chem. Technol. Biotechnol.* **2017**, *92*, 2963.
- [6] H. Rabiee, L. Ge, X. Zhang, S. Hu, M. Li, Z. Yuan, *Energy Environ. Sci.* **2021**, *14*, 1959.
- [7] J. Kintrop, M. Millaruelo, V. Trieu, A. Bulan, E. S. Mojica, *Electrochem. Soc. Interface* **2017**, *26*, 73.
- [8] a) Y. Y. Birdja, E. Pérez-Gallent, M. C. Figueiredo, A. J. Göttle, F. Calle-Vallejo, M. T. M. Koper, *Nat. Energy* **2019**, *4*, 732; b) M. Duarte, B. de Mot, J. Hereijgers, T. Breugelmans, *ChemElectroChem* **2019**, *6*, 5596; c) D. Higgins, C. Hahn, C. Xiang, T. F. Jaramillo, A. Z. Weber, *ACS Energy Lett.* **2019**, *4*, 317; d) J. R. C. Junqueira, P. B. O'Mara, P. Wilde, S. Dieckhöfer, T. M. Benedetti, C. Andronescu, R. D. Tilley, J. J. Gooding, W. Schuhmann, *ChemElectroChem* **2021**, *8*, 4848; e) A. Löwe, M. Schmidt, F. Bienen, D. Kopljär, N. Wagner, E. Klemm, *ACS Sustain. Chem. Eng.* **2021**, *9*, 4213; f) F. Bienen, D. Kopljär, A. Löwe, S. Geiger, N. Wagner, E. Klemm, K. A. Friedrich, *ACS Sustain. Chem. Eng.* **2020**, *8*, 13759; g) N. T. Nesbitt, W. A. Smith, *J. Phys. Chem. C* **2021**, *125*, 13085.
- [9] R. L. Cook, R. C. MacDuff, A. F. Sammells, *J. Electrochem. Soc.* **1990**, *137*, 607.
- [10] N. T. Nesbitt, T. Burdyny, H. Simonson, D. Salvatore, D. Bohra, R. Kas, W. A. Smith, *ACS Catal.* **2020**, *10*, 14093.
- [11] T. Burdyny, W. A. Smith, *Energy Environ. Sci.* **2019**, *12*, 1442.
- [12] L.-C. Weng, A. T. Bell, A. Z. Weber, *Phys. Chem. Chem. Phys.* **2018**, *20*, 16973.
- [13] a) H. Mistry, Y.-W. Choi, A. Bagger, F. Scholten, C. S. Bonifacio, I. Sinev, N. J. Divins, I. Zegkinoglou, H. S. Jeon, K. Kisslinger, E. A. Stach, J. C. Yang, J. Rossmesl, B. Roldan, *Cuenya, Angew. Chem. Int. Ed.* **2017**, *129*, 11552; b) M. Ma, B. J. Trzeźniewski, J. Xie, W. A. Smith, *Angew. Chem. Int. Ed.* **2016**, *128*, 9900.
- [14] a) T. Haas, R. Krause, R. Weber, M. Demler, G. Schmid, *Nat. Catal.* **2018**, *1*, 32; b) R. Krause, D. Reinisch, C. Reller, H. Eckert, D. Hartmann, D. Taroata, K. Wiesner-Fleischer, A. Bulan, A. Lueken, G. Schmid, *Chem. Ing. Tech.* **2020**, *92*, 53; c) S. Verma, X. Lu, S. Ma, R. I. Masel, P. J. A. Kenis, *Phys. Chem. Chem. Phys.* **2016**, *18*, 7075.
- [15] I. Moussallem, J. Jörissen, U. Kunz, S. Pinnow, T. Turek, *J. Appl. Electrochem.* **2008**, *38*, 1177.

- [16] I. Moussallem, S. Pinnow, N. Wagner, T. Turek, *Chem. Eng. Process. Process Intensif.* **2012**, *52*, 125.
- [17] D. Franzen, B. Ellendorff, M. C. Paulisch, A. Hilger, M. Osenberg, I. Manke, T. Turek, *J. Appl. Electrochem.* **2019**, *49*, 705.
- [18] a) N. Sikdar, J. R. C. Junqueira, S. Dieckhöfer, T. Quast, M. Braun, Y. Song, H. B. Aiyappa, S. Seisel, J. Weidner, D. Öhl, C. Andronescu, W. Schuhmann, *Angew. Chem. Int. Ed.* **2021**, *60*, 23427; b) K. Junge Puring, D. Siegmund, J. Timm, F. Möllenbruck, S. Schemme, R. Marschall, U.-P. Apfel, *Adv. Sustainable Syst.* **2021**, *5*, 2000088.
- [19] a) Y. Luo, K. Zhang, Y. Li, Y. Wang, *InfoMat* **2021**, *3*, 1313; b) U. O. Nwabara, E. R. Cofell, S. Verma, E. Negro, P. J. A. Kenis, *ChemSusChem* **2020**, *13*, 855; c) F. Bienen, J. Hildebrand, D. Kopljar, N. Wagner, E. Klemm, K. A. Friedrich, *Chem. Ing. Tech.* **2021**, *93*, 1015; d) M. Li, M. N. Idros, Y. Wu, T. Burdyny, S. Garg, X. S. Zhao, G. Wang, T. E. Rufford, *J. Mater. Chem. A* **2021**, *9*, 19369.
- [20] K. D. Yang, W. R. Ko, J. H. Lee, S. J. Kim, H. Lee, M. H. Lee, K. T. Nam, *Angew. Chem. Int. Ed.* **2017**, *56*, 796.
- [21] a) K. Yang, R. Kas, W. A. Smith, T. Burdyny, *ACS Energy Lett.* **2021**, *6*, 33; b) A. Quinn, R. Sedev, J. Ralston, *J. Phys. Chem. B* **2005**, *109*, 6268.

SUPPORTING INFORMATION

Additional supporting information can be found online in the Supporting Information section at the end of this article.

How to cite this article: P. Wilde, A. Özden, H. Winter, T. Quast, J. Weidner, S. Dieckhöfer, J. R. C. Junqueira, M. Metzner, W. Peter, W. Leske, D. Öhl, T. Bobrowski, T. Turek, W. Schuhmann, *Appl. Res.* **2023**;2:e202200081.
<https://doi.org/10.1002/appl.202200081>